FUDMA Journal of Sciences (FJS)
ISSN online: 2616-1370
ISSN print: 2645 - 2944
Vol. 9 No. 6, June, 2025, pp 375 – 383
DOI: https://doi.org/10.33003/fjs-2025-0906-3730

MAGNETOHYDRODYNAMICS EFFECTS ON STEADY NATURAL CONVECTION COUETTE FLOW OF HEAT GENERATING/ABSORBING FLUID IN A VERTICAL CHANNEL WITH VISCOUS DISSIPATION

Kabir M. Tafida, Aisha Y. Abdullahi and Nura Auwal

Department of Mathematics Federal University of Education, Zaria, Nigeria

*Corresponding authors' email: mktafida.555@gmail.com

ABSTRACT
This study investigates the impact of magnetohydrodynamics (MHD) on steady natural convection Couette flow of a heat generating/absorbing fluid in a vertical channel in the presence of viscous dissipation. The dimensionless governing equations for momentum and energy were analytically solved using the Homotopy perturbation method. The influence of various physical parameters on the flow behavior is illustrated through graphical results. Moreover, the effects of these parameters on skin friction, rate of heat transfer, mass flux and mean temperature are analyzed and presented numerically in tabular form. Findings from the study show that, the magnetic field intensity on the velocity and temperature distributions of the fluid. It is worth highlighting that increasing the permeability enhances the fluid velocity and also the temperature near the heated plate rises, while a steeper temperature gradient is observed across the channel. Increasing the Eckert number significantly enhances both fluid velocity and temperature. The findings of this study are important due to its application in magnetohydrodynamics Power Generation, Metallurgy and Materials Processing, Cooling Systems in Nuclear Reactors, Electromagnetic Pumps, Plasma Propulsion and Aerospace and Food and Chemical Industries.

Keywords: Magnetic field, Heat generation/absorption, Homotopy perturbation method, Permeability, Viscous dissipation

INTRODUCTION
The study of magnetohydrodynamic (MHD) steady natural convection Couette flow with heat transfer in a vertical parallel channel has garnered significant attention in recent literature. These types of flows are prevalent in various industrial processes and natural phenomena, including geothermal energy extraction, nuclear waste management, groundwater flow, industrial and agricultural water systems, oil recovery, thermal insulation, pollutant transport in aquifers, cooling of electronic devices, packed bed reactors, and food processing. Numerous researchers have explored MHD flow in channels. Razaa *et al.* (2023) observed that fluid temperature rises with increased viscous dissipation. Jha and Aina (2017) found that accounting for the induced magnetic field leads to higher velocity profiles compared to when it is neglected. Omokhuale and Dange (2023) reported that an increase in magnetic field strength hinders fluid motion due to the Lorentz force. Ajibade and Tafida (2019a) emphasized the critical role of viscous dissipation in natural convection and recommended its inclusion in future studies. Akbar *et al.* (2022) demonstrated that fluid energy grows substantially with higher viscous dissipation. Waini *et al.* (2023) showed that a higher Eckert number reduces the heat transfer rate. Ajibade and Tafida (2019b) also noted that fluid velocity increases near the heated surface with a rise in the heat generation parameter. Hassan *et al.* (2022) concluded that both heat generation and absorption reduce the momentum boundary layer thickness. Usman (2024) found that stronger magnetic parameters enhance the Lorentz force, which opposes fluid motion within the boundary layer. Oni and Jha (2019) discovered that heat generation increases, while heat absorption decreases, both temperature and velocity distributions.

Tafida *et al.* (2023) observed that fluid velocity decreases as the magnetic field parameter increases. Ramesh (2018) noted that fluid temperature rises consistently with increasing viscous dissipation. Eswaran and Kumar (2025) emphasized flow velocity, while an increase in the magnetic parameter reduces it. Similarly, Ajibade *et al.* (2024) observed that that understanding the influence of the magnetic parameter on fluid flow can contribute to better system design and optimization. Alam *et al.* (2018) found that increasing the magnetic field parameter results in lower velocity profiles but higher temperature profiles. Similarly, Hamza *et al.* (2024) reported that increasing the magnetic field strength leads to a reduction in fluid velocity. Jha and Samaila (2022) concluded that heat generation acts as a thermal resistance, impeding heat transfer from the left plate to the right plate. Tafida *et al.* (2024) observed that fluid velocity increases near the heated plate but decreases near the cold plate with greater viscous dissipation. In contrast, Kaita *et al.* (2024) found that fluid velocity increases with a rise in the magnetic field parameter. Zigta (2022) concluded that the temperature profile of a micropolar fluid decreases with an increase in the Prandtl number. Srisailam *et al.* (2023) demonstrated that while higher magnetic field values elevate the energy profile, they concurrently reduce the velocity profile.

Ajibade and Tafida (2020) found that both fluid temperature and velocity increase with higher heat generation, while they decrease with greater heat absorption. Mishra *et al.* (2023) observed that fluid velocity rises with increasing values of the magnetic field parameter. Kumar *et al.* (2023) reported that a rise in the Grashof number enhances buoyancy forces, which in turn intensifies fluid flow under heat generation and absorption conditions. Oni and Jha (2023) concluded that both skin friction and the rate of heat transfer are sensitive to variations in the heat generation/absorption parameter. Tafida and Tajuddeen (2024) emphasized that the Homotopy Perturbation Method provides a straightforward and effective approach for solving coupled and nonlinear differential equations. Nabwey *et al.* (2024) showed that magnetic permeability also influences the temperature distribution within the material. Shabiha and Tamizharasi (2025) found that fluid velocity decreases as the magnetic field strength increases. Sekhar (2023) noted that higher values of the permeability and heat generation parameters enhance fluid greater material permeability results in increased fluid velocity. Chillingo *et al.* (2024) observed that an increase in the permeability parameter leads to a gradual reduction in the fluid velocity profile.

Gouder et al. (2022) emphasized the Homotopy Perturbation Method (HPM) as a promising approach for wave equations. Similarly, Jassim and Mohammed (2021) found the method to be straightforward to implement while delivering accurate results. Sobamowo (2023) demonstrated Homotopy perturbation method capability to determine complex roots of nonlinear equations, while Khaleghizadeh (2022) affirmed its power and efficiency in tackling nonlinear problems. Farhood and Mohammed (2023) further noted that HPM is highly effective and enhances the rapid convergence of solutions through its simplicity.

In light of the reviewed literature, it is evident that further investigation into steady MHD natural convection flow and heat transfer in a vertical channel, particularly involving a heat-generating or absorbing fluid with viscous dissipation, is of considerable importance. This study aims to examine the effects of magnetohydrodynamics on steady natural convection Couette flow of such a fluid within a vertical channel, accounting for the influence of viscous dissipation. The governing equations are analytically solved using the Homotopy Perturbation Method. Graphical representations are provided to illustrate the impact of key physical parameters, while results for skin friction, heat transfer rate, mass flux, and mean temperature are presented in tabular form. The present investigation could be utilized in the food processing and preservation industries, as well as in fuel drilling and power generation sectors.

MATERIALS AND METHODS

Consider a steady fully developed laminar flow of a magnetohydrodynamic (MHD), viscous, incompressible and electrically conducting fluid, influenced by heat generation or absorption, viscous dissipation and a transverse magnetic field. One boundary plate remains stationary at ambient temperature while the opposing plate is heated and moves at a constant velocity$U$. The fluid is assumed to have constant physical properties throughout the flow domain.

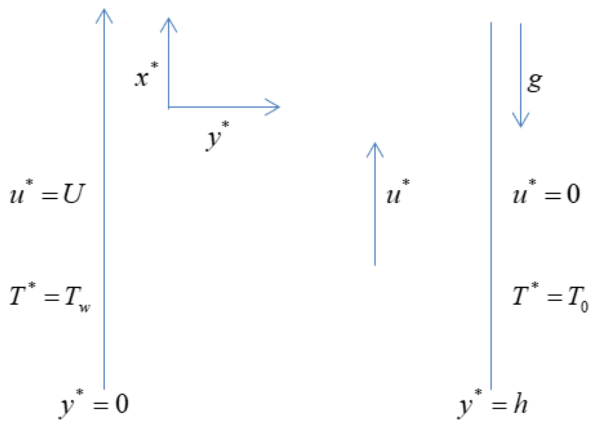

Figure 1: Diagrammatic representation of the problem

The dimensional governing equations for momentum and energy are derived under the framework of the Boussinesq approximation and are expressed as follows:

$$\nu \frac{d^2u^*}{dy^{*2}} - \left(\frac{\sigma B_0^2}{\rho} + \frac{\nu}{k^*}\right)u^* + g\beta(T^* - T_0) = 0, \tag{1}$$

$$k\frac{d^2T^*}{dy^{*2}} - Q_0(T^* - T_0) + \mu\left(\frac{du^*}{dy^*}\right)^2 = 0, \tag{2}$$

Here ν denotes the kinematic viscosity, u^* indicates the dimensional velocity, y^* refers to the dimensional distance, B_0 signifies the magnetic induction, β stands for the coefficient of thermal expansion, T^* represents the fluid temperature (in dimensional form), T_0 refers to the ambient temperature, k denotes the thermal conductivity, Q_0 is the coefficient of heat generation or absorption, ρ represents the fluid density, μ is the viscosity coefficient and g represents the acceleration due to gravity.

The system is subject to the following boundary conditions:

$$u^* = U, T^* = T_w \text{ at } y^* = 0,$$
$$u^* = 0, T^* = T_0 \text{ at } y^* = h. \tag{3}$$

Here, U denotes the velocity of the moving plate, T_w represents the temperature of the heated plate, and T_0 indicates the temperature of the cold plate. The dimensionless parameters used in equations (1) and (2) along with the boundary condition specified in equation (3), are defined as follows.

$$y = \frac{y^*}{h}, u = \frac{u^*}{U}, Ec = \frac{U_0}{cp(T_w - T_0)}, T = \frac{T^* - T_0}{T_w - T_0},$$

$$Pr = \frac{\nu}{\alpha}, Gr = \frac{g\beta h^2(T_w - T_0)^2}{\nu U_0}, S = \frac{Q_0 h}{k}. \tag{4}$$

Where y represents the non-dimensional temperature, u denotes the non-dimensional velocity, Pr is the Prandtl number, S refers to the non-dimensional heat generation/absorption parameter and Gr is the non-dimensional thermal Grashof number, respectively.

The governing momentum and energy equations (1) and (2) together with the boundary condition (3) are converted into their dimensionless form using the dimensionless equation (4) as shown below:

$$\frac{d^2u}{dy^2} - \left(M + \frac{1}{K}\right)u + GrT = 0, \tag{5}$$

$$\frac{d^2T}{dy^2} + Ec\,Pr\left(\frac{du}{dy}\right)^2 - ST = 0, \tag{6}$$

The associated boundary conditions are as follows:

$$u = 1, T = 1 \text{ at } y = 0,$$
$$u = 0, T = 0 \text{ at } y = 1. \tag{7}$$

Homotopy Perturbation Method

Using a convex homotopy, the momentum and energy equations (5) and (6), together with the boundary condition (7), are solved via the Homotopy perturbation method as outlined below:

$$H(u,p) = (1-p)\left(\frac{d^2u}{dy^2}\right) + p\left(\frac{d^2u}{dy^2} - \left(M + \frac{1}{K}\right)u + GrT\right) = 0, \tag{8}$$

$$H(T,p) = (1-p)\left(\frac{d^2T}{dy^2}\right) + p\left(\frac{d^2T}{dy^2} + Ec\,Pr\left(\frac{du}{dy}\right)^2 - ST\right) = 0. \quad (9)$$

Accordingly, when no initial approximation is provided, the equation assumes the following form:

$$\frac{d^2u}{dy^2} = p\left(\left(M + \frac{1}{K}\right)u - GrT\right) \quad (10)$$

$$\frac{d^2T}{dy^2} = p\left(-Ec\,Pr\left(\frac{du}{dy}\right)^2 + ST\right) \quad (11)$$

The solutions of equations (5) and (6) are expressed in the following form:

$$u = u_0 + pu_1 + p^2u_2 + p^3u_3 + \ldots, \quad (12)$$

$$T = T_0 + pT_1 + p^2T_2 + p^3T_3 + \ldots, \quad (13)$$

Substituting equation (12) into equation (10) and equation (13) into equation (11) yields the following results

$$:\frac{d^2u_0}{dy^2} + p\frac{d^2u_1}{dy^2} + p^2\frac{d^2u_2}{dy^2} + \ldots = p\left(\left(M + \frac{1}{K}\right)u_0 - GrT_0\right) + p^2\left(\left(M + \frac{1}{K}\right)u_1 - GrT_1\right) + p^3\left(\left(M + \frac{1}{K}\right)u_2 - GrT_2\right) + \ldots \quad (14)$$

$$\frac{d^2T_0}{dy^2} + p\frac{d^2T_1}{dy^2} + p^2\frac{d^2T_2}{dy^2} + \ldots = p\left(-Ec\,Pr\left(\frac{du_0}{dy}\right)^2 + ST_0\right) + p^2\left(-2Ec\,Pr\frac{du_0}{dy}.\frac{du_1}{dy} + ST_1\right) + p^3\left(-2Ec\,Pr\frac{du_0}{dy}.\frac{du_2}{dy} - Ec\,Pr\left(\frac{du_1}{dy}\right)^2 + ST_2\right) + \ldots \quad (15)$$

Equating the coefficients of the corresponding terms p^0, p^1, p^2 and p^3 in equations (14) and (15) gives:

$$p^0: \frac{d^2u_0}{dy^2} = 0, \quad (16)$$

$$p^0: \frac{d^2T_0}{dy^2} = 0, \quad (17)$$

$$p^1: \frac{d^2u_1}{dy^2} = \left(M + \frac{1}{K}\right)u_0 - GrT_0, \quad (18)$$

$$p^1: \frac{d^2T_1}{dy^2} = -Ec\,Pr\left(\frac{du_0}{dy}\right)^2 + ST_0, \quad (19)$$

$$p^2: \frac{d^2u_2}{dy^2} = \left(M + \frac{1}{K}\right)u_1 - GrT_1, \quad (20)$$

$$p^2: \frac{d^2T_2}{dy^2} = -2Ec\,Pr\left(\frac{du_0}{dy}.\frac{du_1}{dy}\right) + ST_1, \quad (21)$$

$$p^3: \frac{d^2u_3}{dy^2} = \left(M + \frac{1}{K}\right)u_2 - GrT_2, \quad (22)$$

$$p^3: \frac{d^2T_3}{dy^2} = -2Ec\,Pr\left(\frac{du_0}{dy}.\frac{du_2}{dy}\right) - Ec\,Pr\left(\frac{du_1}{dy}\right)^2 + ST_2. \quad (23)$$

The boundary condition given in equation (7) is reformulated as:

$$\left.\begin{array}{l} u_0(0) = 1, u_1(0) = u_2(0) = u_3(0) = \ldots = 0, \\ u_0(1) = u_1(1) = u_2(1) = u_3(1) = \ldots = 0, \\ T_0(0) = 1, T_1(0) = T_2(0) = T_3(0) = \ldots = 0, \\ T_0(1) = T_1(1) = T_2(1) = T_3(1) = \ldots = 0. \end{array}\right\} \quad (24)$$

By applying equations (16) and (17) in conjunction with the boundary conditions $u_0(0) = 1$ and $u_0(1) = 0$, $T_0(0) = 1$ and $T_0(1) = 0$performing the necessary computations, equations (25) and (26) are derived as follows:

$$u_0 = A_1y + A_2, \quad (25)$$

$$T_0 = B_1y + B_2. \quad (26)$$

By applying equations (18) and (19) in conjunction with the boundary conditions $u_1(0) = 0$and $u_1(1) = 0$, $T_1(0) = 0$and $T_1(1) = 0$ performing the necessary computations, equations (27) and (28) are derived as follows:

$$u_1 = \left(M + \frac{1}{K}\right)\left(\frac{y^2}{2} - \frac{y^3}{6}\right) - Gr\left(\frac{y^2}{2} - \frac{y^3}{6}\right) + A_3y + A_4, \quad (27)$$

$$T_1 = -\frac{Ec\,Pr\,y^2}{2} + S\left(\frac{y^2}{2} - \frac{y^3}{6}\right) + B_3y + B_4. \quad (28)$$

By applying equations (20) and (21) in conjunction with the boundary conditions $u_2(0) = 0$and $u_2(1) = 0$, $T_2(0) = 0$and $T_2(1) = 0$ performing the necessary computations, equations (29) and (30) as follows:

$$u_2 = \left(M + \frac{1}{K}\right)^2\left(\frac{y^4}{24} - \frac{y^5}{120}\right) - Gr\left(M + \frac{1}{K}\right)\left(\frac{y^4}{24} - \frac{y^5}{120}\right) + \left(M + \frac{1}{K}\right)\frac{A_3y^3}{6} + \frac{Ec\,Pr\,Gry^4}{24} - GrS\left(\frac{y^4}{24} - \frac{y^5}{120}\right) - \frac{GrB_3y^3}{6} + A_5y + A_6, \quad (29)$$

$$T_2 = Ec\,Pr\,G\,r\left(M + \frac{1}{K}\right)\left(\frac{y^3}{3} - \frac{y^4}{12}\right) - Ec\,Pr\,G\,r\left(\frac{y^3}{3} - \frac{y^4}{12}\right) + Ec\,Pr\,A_3\,y^2 - \frac{Ec\,Pr\,Sy^4}{24} + S^2\left(\frac{y^4}{24} - \frac{y^5}{120}\right) + \frac{SB_3y^3}{6} + B_5y + B_6, \quad (30)$$

where,

$A_1 = B_1 = -1,$

$A_2 = B_2 = 1,$

$A_3 = \frac{Gr}{3} - \frac{1}{3}\left(M + \frac{1}{K}\right), \quad A_4 = 0,$

$B_3 = \frac{EcPr}{2\frac{S}{3}} \quad B_4 = 0,$

$A_5 = -\frac{1}{30}\left(M + \frac{1}{K}\right)^2 + \frac{Gr}{30}\left(M + \frac{1}{K}\right) - \frac{A_3}{6}\left(M + \frac{1}{K}\right) - \frac{Ec\,Pr\,Gr}{24} + \frac{GrS}{30} + \frac{GrB_3}{6},$

$B_5 = \frac{Ec\,Pr\,Gr}{4} - \frac{EcPr}{4}\left(M + \frac{1}{K}\right) - EcPr\,A_3 + \frac{Ec\,Pr\,S}{24} - \frac{S^2}{30} - \frac{SB_3}{6}$

$A_6 = B_6 = 0.$

Equations (25) - (30) give the approximate solutions for velocity and temperature as:

$$u = u_0 + u_1 + u_2 + \ldots, \quad (31)$$

$$T = T_0 + T_1 + T_2 + \ldots. \quad (32)$$

The skin friction at the channel fluid boundary surfaces is determined by differentiating equation (31) with respect to y and evaluated at the boundaries $y = 0$and $y = 1$ as follows:

$$\tau_0 = \left.\frac{du}{dy}\right|_{y=0} = -1 + A_3 + A_5, \quad (33)$$

$$\tau_1 = \left.\frac{du}{dy}\right|_{y=1} = -1 + \frac{1}{2}\left(M + \frac{1}{K}\right) - \frac{Gr}{2} + A_3 + \frac{1}{8}\left(M + \frac{1}{K}\right)^2 - \frac{Gr}{8}\left(M + \frac{1}{K}\right) + \frac{A_3}{2}\left(M + \frac{1}{K}\right) + \frac{EcPr}{6\frac{GrSGrB_3}{8\;\;2\;\;5}} \quad (34)$$

The heat transfer rate at the channel fluid boundary surfaces is determined by differentiating equation (32) with respect to y and evaluated at the boundaries $y = 0$ and $y = 1$ as follows:

$$Nu_0 = \left.\frac{dT}{dy}\right|_{y=0} = -1 + B_3 + B_5, \quad (35)$$

$$Nu_1 = \left.\frac{dT}{dy}\right|_{y=1} = -1 - Ec\,Pr + \frac{SB_3}{2} + \frac{2EcPr}{3\left(M+\frac{1}{K}\right)\frac{2Ec\,Pr\,Gr}{3}} + 2Ec\,Pr\,A_3 - \frac{Ec\,Pr\,S}{6} + \frac{S^2}{8} + \frac{SB_3}{2} + B_5. \quad (36)$$

Using the expression for mass flux $Q_m = \int_0^1 u(y)dy$, we derive:

$$Q_m = \frac{1}{2} + \frac{1}{2}\left(M + \frac{1}{K}\right) - \frac{Gr}{8} + \frac{A_3}{2} + \frac{1}{144}\left(M + \frac{1}{K}\right)^2 - \frac{Gr}{144}\left(M + \frac{1}{K}\right) + \frac{A_3}{24}\left(M + \frac{1}{K}\right) + \frac{Ec\,Pr\,Gr}{120} - \frac{GrS}{144} - \frac{GrB_3}{24} + \frac{A_5}{2}, \quad (37)$$

In a similar manner, the mean temperature is expressed as:

$$\theta_m = -\frac{1}{3} - \frac{7EcPr}{24} + \frac{13S}{60} + \frac{5B_3}{6} + \frac{1}{30}\left(M + \frac{1}{K}\right) - \frac{13EcPr}{360}\left(M + \frac{1}{K}\right)\frac{A_3}{6} + \frac{S}{65}\left(M + \frac{1}{K}\right) + \frac{B_3}{8}\left(M + \frac{1}{K}\right) - \frac{Gr}{30} + \frac{13Ec\,Pr\,Gr}{360} + \frac{GrS}{64} - \frac{11GrB_3}{120} - \frac{Ec\,Pr\,A_3}{8} + \frac{11AS}{120} + \frac{A_3B_3}{3}. \quad (38)$$

RESULTS AND DISCUSSION

This study investigates a magnetohydrodynamic natural convection model characterized by several fundamental physical parameters, such as viscous dissipation, Prandtl number, Grashof number, heat generation or absorption, magnetic field and permeability. The effects of these parameters on velocity and temperature distributions are depicted through graphical illustrations. Furthermore, numerical values for skin friction, heat transfer rate, mass flux and mean temperature are presented in tabular form for comprehensive analysis

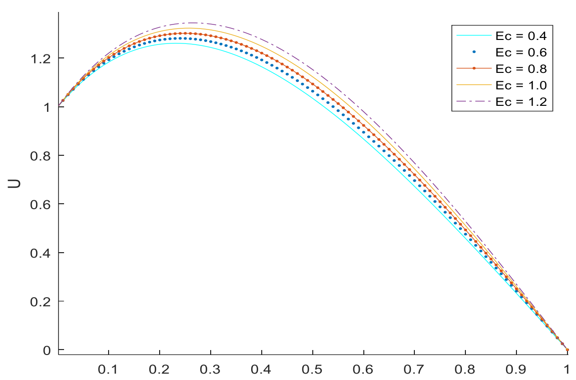

Figure 2: Velocity profile for different values of Ec when $Gr = 6.0, Pr = 0.71, M = 0.4, S = 1.0$ and $K = 0.4$.

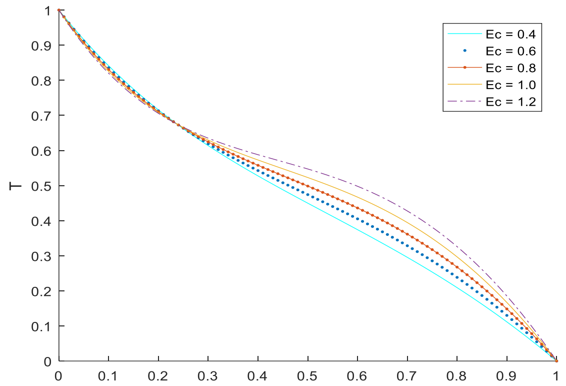

Figure 3: Temperature profile for different values of Ec when $Gr = 6.0, Pr = 0.71, M = 0.4, S = 1.0$ and $K = 0.4$

As depicted in Figures 2 and 3, increasing the Eckert number significantly enhances both fluid velocity and temperature, primarily as a result of intensified viscous dissipation. This phenomenon mitigates the damping effects imposed by the magnetic field and exemplifies the behavior of thermo-fluid systems where internal energy transformation plays a crucial role in governing flow characteristics. The resulting temperature rise amplifies buoyant forces, thereby promoting greater fluid acceleration. Additionally, a higher Eckert number augments internal heat generation, leading to elevated temperature levels throughout the boundary layer. In essence, increased viscous dissipation facilitates a more efficient conversion of kinetic energy into thermal energy.

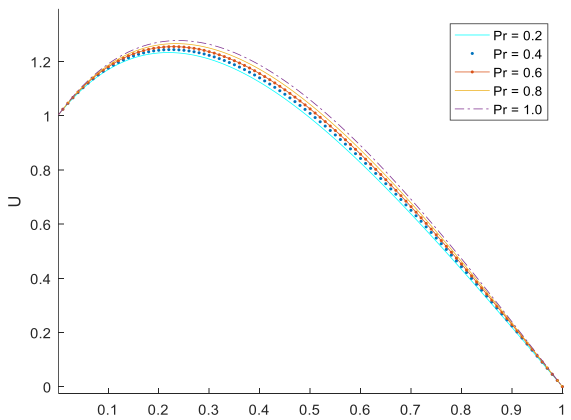

Figure 4: Velocity profile for different values of Pr when $Ec = 0.4, Gr = 6.0, M = 0.4, S = 1.0$ and $K = 0.4$.

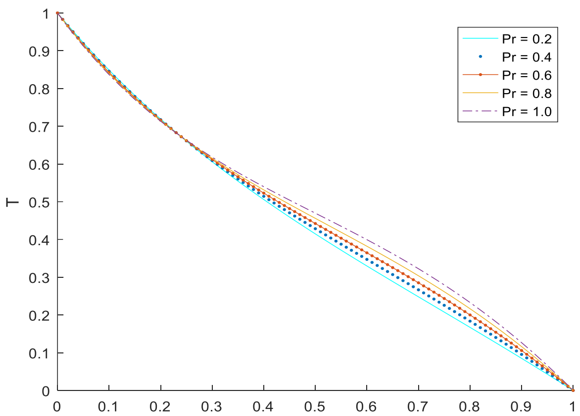

Figure 5: Temperature profile for different values of Pr when $Ec = 0.4, Gr = 6.0, M = 0.4, S = 1.0$ and $K = 0.4$.

Figures 4 and 5 illustrate the velocity and temperature profiles, respectively, for different values of the Prandtl number. From Figure 4, it is evident that an increase in the Prandtl number leads to a slight rise in the velocity profile, with the peak shifting upward before gradually declining toward the wall. This trend can be attributed to the reduced thermal diffusivity associated with higher Prandtl numbers, which allows heat to remain in the fluid for a longer duration, thereby intensifying the buoyancy effect and enhancing fluid motion. In Figure 5, it is observed that as the Prandtl number increases, the temperature near the heated wall becomes higher, while the temperature drops more sharply across the channel. This indicates that higher Prandtl numbers result in steeper temperature gradients due to the lower thermal conductivity of the fluid.

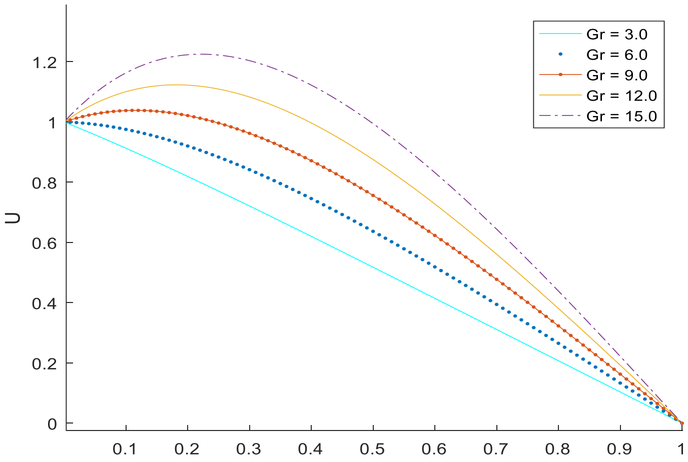

Figure 6: Velocity profile for different values of Gr when $Ec = 0.4, Pr = 0.71, M = 0.4, S = 1.0$ and $K = 0.4$.

Figure 6 illustrates the influence of the Grashof number on fluid velocity. It can be observed that an increase in the Grashof number leads to a notable rise in fluid velocity, attributed to the intensification of buoyancy driven forces. In practical applications where natural convection governs the flow, modifying parameters that affect the Grashof number, such as fluid properties or temperature gradients serves as a practical strategy to enhance both flow dynamics and heat transfer efficiency.

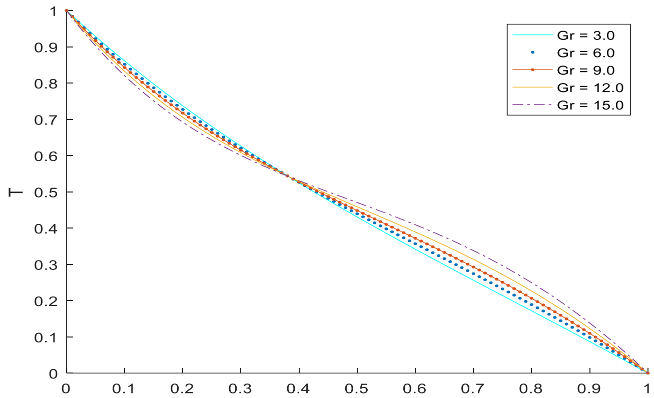

Figure 7: Temperature profile for different values of Gr when $Ec = 0.4, Pr = 0.71, M = 0.4, S = 1.0$ and $K = 0.4$.

Figure 7 depicts the corresponding effect on the temperature profile. As the Grashof number increases, the temperature field becomes more diffused, indicating stronger convective heat transport and the maintenance of elevated temperatures at greater distances from the heated surface.

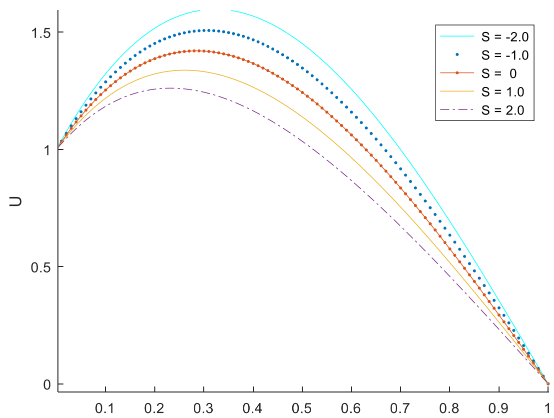

Figure 8: Velocity profile for different values of S when $Ec = 0.4, Pr = 0.71, Gr = 6.0, M = 0.4$ and $K = 0.4$.

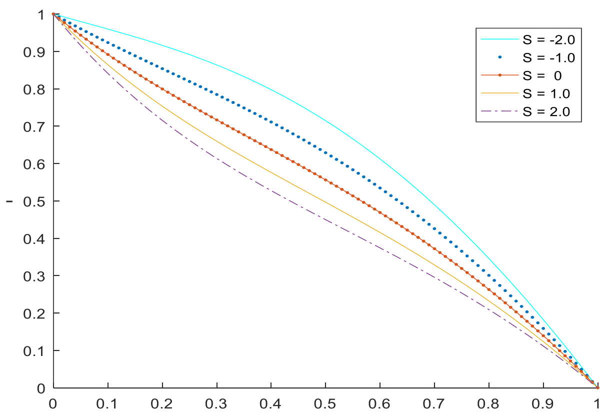

Figure 9: Temperature profile for different values of S when $Ec = 0.4, Pr = 0.71, Gr = 6.0, M = 0.4$ and $K = 0.4$.

Figures 8 and 9 illustrate the impact of heat generation and absorption on the velocity and temperature profiles. As heat generation increases, both the fluid temperature and velocity rise. Conversely, increased heat absorption results in a reduction of these parameters. This decline is attributed to the drop in fluid temperature, which leads to a thinner thermal boundary layer and a corresponding decrease in fluid velocity. On the other hand, higher heat generation elevates the temperature and velocity distributions, contributing to a thicker thermal boundary layer and enhancing the fluid's convective flow. In addition, increased heat generation boosts both temperature and fluid motion, thereby amplifying convective heat transfer mechanisms.

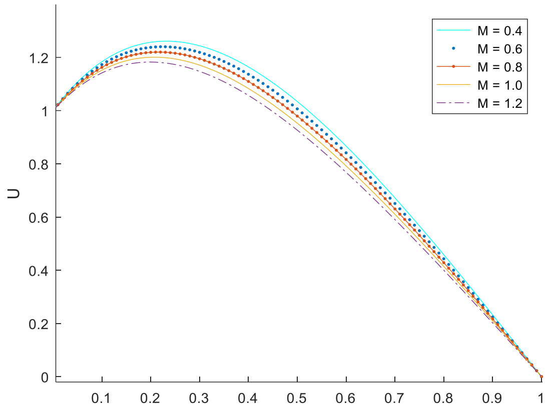

Figure 10: Velocity profile for different values of M when $Ec = 0.4, Pr = 0.71, Gr = 6.0, S = 1.0$ and $K = 0.4$.

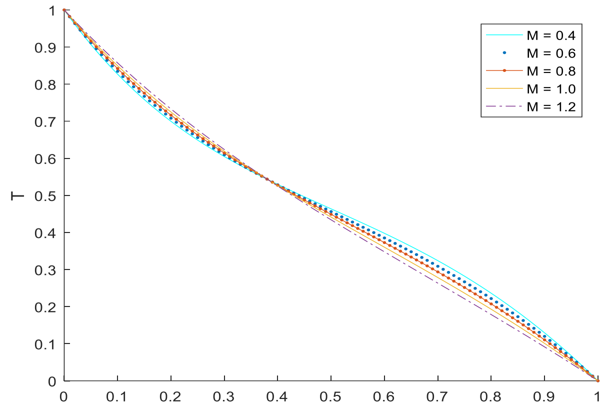

Figure 11: Temperature profile for different values of M when $Ec = 0.4, Pr = 0.71, Gr = 6.0, S = 1.0$ and $K = 0.4$.

Figures 10 and 11 depict the effect of magnetic field intensity on the velocity and temperature distributions of the fluid. Figure 10 demonstrates that fluid velocity increases as the magnetic field strength rises. This behavior aligns with physical reasoning, as a stronger magnetic field amplifies the Lorentz force, which resists fluid motion and consequently elevates the velocity. Furthermore, an increase in magnetic field strength leads to a rise in fluid temperature near the heated plate, while a reduction in temperature is observed near the cold plate.

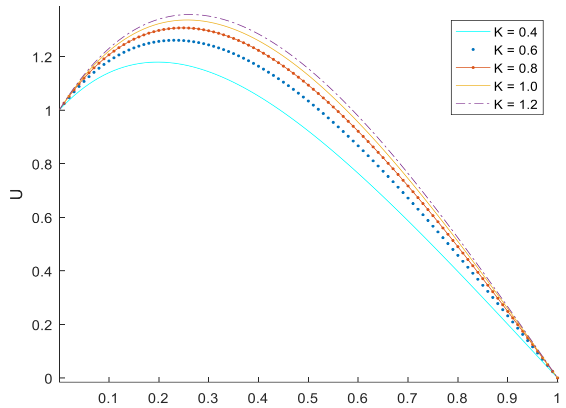

Figure 12: Velocity profile for different values of K when $Ec = 0.4, Pr = 0.71, Gr = 6.0, S = 1.0$ and $M = 0.4$.

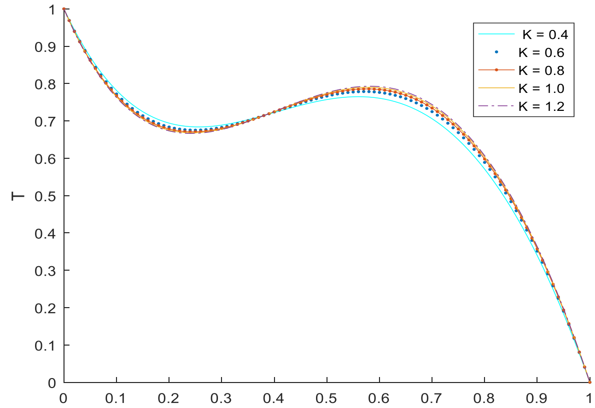

Figure 13: Temperature profile for different values of K when $Ec = 0.4, Pr = 0.71, Gr = 6.0, S = 1.0$ and $M = 0.4$.

The influence of permeability parameter on velocity and temperature are depicted in Figures 12 and 13 illustrate the effect of the permeability parameter Kon the fluid velocity and temperature profiles. As shown in Figure 12, increasing the permeability enhances the fluid velocity, as higher permeability facilitates freer movement of fluid particles, thereby promoting greater flow. Figure 13 demonstrates that with increasing permeability, the temperature near the heated plate rises, while a steeper temperature gradient is observed across the channel.

Table 1: Estimated Numerical Values of skin Friction at the Plate $y = 0$ and $y = 1$

	$(Ec = 0.2, K = 0.4, M = 1.0)$		$(Ec = 0.2, K = 0.4, M = 2.0)$		$(Ec = 0.4, K = 0.8, M = 2.0)$	
S	τ_0	τ_1	τ_0	τ_1	τ_0	τ_1
−1.0	0.43650	0.24321	0.41967	0.22034	1.34662	1.19890
−0.5	0.46704	0.25018	0.44281	0.23551	1.36414	1.21739
0	0.47132	0.27664	0.46300	0.25920	1.39001	1.40818
0.5	0.50167	0.29541	0.48421	0.27684	1.41238	1.69200
1.0	0.53103	0.31282	0.50132	0.29965	1.42998	1.80412

Table 1 illustrates the variation in skin friction between the fluid and the bounding plates. It is observed that an increase in magnetic field strength leads to a reduction in skin friction on both plates. This behavior is consistent with physical expectations, as a stronger magnetic field intensifies the Lorentz force, which acts against the fluid motion, thereby diminishing skin friction. Furthermore, the data indicate that skin friction increases with greater viscous dissipation and higher permeability of the medium. Lastly, skin friction is found to rise with enhanced heat absorption, while it decreases in response to increased heat generation.

Table 2: Estimated numerical values of rate of heat transfer at the plate $y = 0$ and $y = 1$

S	$(Ec = 0.2, K = 0.4, M = 1.0)$		$(Ec = 0.2, K = 0.4, M = 2.0)$		$(Ec = 0.4, K = 0.8, M = 2.0)$	
	Nu_0	Nu_1	Nu_0	Nu_1	Nu_0	Nu_1
-1.0	1.44640	1.33314	1.43092	1.31114	1.57211	1.62013
-0.5	1.44042	1.35012	1.42901	1.32915	1.54013	1.64193
0	1.42125	1.38864	1.40311	1.33202	1.51071	1.67010
0.5	1.40307	1.39997	1.38121	1.35104	1.48216	1.69982
1.0	1.38201	1.40512	1.37426	1.37252	1.45813	1.72236

Table 2 highlights the rate of heat transfer between the fluid and the plates. The results indicate that an increase in magnetic field strength suppresses the heat transfer rate on both plates. In contrast, higher values of viscous dissipation and permeability lead to an enhancement in heat transfer. The data further reveal that heat absorption increases the heat transfer rate on the moving plate, whereas a reduction is observed on the stationary plate. On the other hand, increasing heat generation results in a decline in heat transfer on the moving plate, but an increase on the stationary plate. This contrasting behavior is attributed to the movement of high energy fluid particles from the moving plate toward the stationary plate, which raises the fluid temperature in the vicinity of the stationary surface.

Table 3: Estimated numerical values of mass flux Q

S	$(Ec = 0.2, K = 0.4, M = 1.0)$ Q	$(Ec = 0.2, K = 0.4, M = 2.0)$ Q	$(Ec = 0.4, K = 0.8, M = 2.0)$ Q
-1.0	0.47716	0.49241	0.53056
-0.5	0.49562	0.52087	0.55501
0	0.53281	0.55470	0.58109
0.5	0.55815	0.57805	0.60411
1.0	0.57611	0.59257	0.63055

Table 3 provides the numerical values of mass flux$Q$. The results reveal that an increase in magnetic field strength leads to an enhancement in mass flux. Additionally, higher values of viscous dissipation and permeability are associated with increased mass flux. Moreover, heat absorption is found to promote mass flux, while heat generation has the opposite effect causing a reduction.

Table 4: Estimated numerical values of mean temperature θ_m

S	$(Ec = 0.2, K = 0.4, M = 1.0)$ θ_m	$(Ec = 0.2, K = 0.4, M = 2.0)$ θ_m	$(Ec = 0.4, K = 0.6, M = 2.0)$ θ_m
-1.0	0.42105	0.42892	0.49164
-0.5	0.37961	0.38861	0.44591
0	0.35234	0.35912	0.41602
0.5	0.32398	0.33239	0.39101
1.0	0.31056	0.31786	0.36231

Table 4 presents the numerical values for the mean temperature. It is evident that both viscous dissipation and the permeability parameter contribute to an increase in mean temperature, reflecting their role in converting mechanical energy into thermal energy. Moreover, the mean temperature rises with an increase in heat generation, whereas the opposite effect is observed with heat absorption.

Validation

Table 5: Validation of present problem and that of Ajibade and Tafida (2019a)

S	Ajibade and Tafida (2019a) $Ec = 0.4, Pr = 0.71, Gr = 8.0, y = 0.5.$		Present Problem $Ec = 0.4, Pr = 0.71, Gr = 8.0, y = 5.0, M = 0, K = 1000$	
	Velocity	Temperature	Velocity	Temperature
-1.0	1.06415	0.56833	1.06407	0.56827
-0.5	1.02906	0.53502	1.02914	0.53513
0.5	0.97528	0.47038	0.97516	0.47025
1.0	0.95398	0.44349	0.95385	0.44335

For numerical validation of the present problem, the computed results for velocity and temperature are compared with the published work of Ajibade and Tafida (2019a), as presented in Table 5. A good agreement is observed when the magnetic field is neglected and the permeability parameter is assumed to be sufficiently large.

CONCLUSION

This study presents a mathematical analysis and solution of steady MHD natural convection Couette flow of an incompressible fluid within vertical channels. The dimensionless governing momentum and energy equations are solved using the homotopy perturbation method. The influence of various dimensionless parameters on the flow characteristics is illustrated and analyzed through graphical representations. The results show excellent agreement with the findings of Ajibade and Tafida (2019a). The key conclusions of this investigation are summarized as follows:

i. An increase in the Eckert number leads to a significant rise in both fluid velocity and temperature.
ii. Increased heat generation results in elevated temperature and velocity profiles,
iii. An increase in magnetic field strength enhances fluid velocity and raises the temperature near the heated plate,
iv. Higher permeability increases fluid velocity and also elevates the temperature near the heated plate,
v. An increase in magnetic field strength reduces the heat transfer rate on both plates,
vi. Finally, magnetic field and permeability are essential fluid properties, and their incorporation into the fluid flow equations plays a key role in shaping the flow dynamics and thermodynamic characteristics within the channel

REFERENCES

Ajibade, A. O. and Tafida, M. K. (2019a). Viscous dissipation effect on steady natural convection Couette flow of heat generating fluid in a vertical channel. Journal of Advances in Mathematics and Computer Science. 30(1): 1 – 16. https://doi.org/10.9734/JAMSC/2019/45020.

Ajibade, A. O. and Tafida, M. K. (2019b). Viscous dissipation effect on a steady generalised Couette flow of heat-generating/absorbing fluid in a vertical channel. Z. Naturforsch. 74(7)a: 605 – 616. https://doi.org/10.1515/zna-2018-0537

Ajibade, A. O. and Tafida, M. K. (2020). The combined effect of variable viscosity and variable thermal conductivity on natural convection Couette flow. International Journal of Thermofluids. 100036, 5 – 6. https://doi.org/10.1016/j.ijft.2020.100036

Ajibade, A. O., Gambo, J. J. and Jha, B. K. (2024). Effects of Darcy and viscous dissipation on natural convection flow in a vertical tube partially filled with porous material under convective boundary condition. Int. J. Appl. Comput. Math. 10:84. https://doi.org/10.1007/s40819-023-01623-2.

Akbar, N., Hussain, S.M. and Khan, R.U. (2022). Numerical solution of Casson fluid flow under viscous dissipation and radiation phenomenon. Journal of Applied Mathematics and Physics, 10: 475 - 490. https://doi.org/10.4236/jamp.2022.102036

Alam, Md. M., Begum, R., Islam, M. M. and Parvez, M. M. (2018). Numerical study of temperature dependent viscosity and thermal conductivity on a natural convection flow over a sphere in presence of magneto hydrodynamics. Current Journal of Applied Science and Technology. 28(4): 1 – 13. https://doi.org/10.9734/CJAST/2018/42677

Chillingo, K. J., Mng'ang'a, J., Onyango, E. R. and Matoa, M. (2024). Influence of induced Mgnetic field and chemically reacting on hydromagnetic Couette flow of Jeffrey fluid in an inclined channel with variable viscosity and convective cooling: A caputo derivative approach. 22: 100627.

Eswaran, R. and Jagadeesh-Kumar, M. S. (2025). Influence of MHD flow on forced convection in a saturated porous duct with Ohmic heating. Discover Applied Sciences. 7:36. https://doi.org/10.1007/s42452-024-06432-w

Farhood, A. K. and Mohammed, O. H. (2023). Homotopy Perturbation Method for solving time-fractional nonlinear variable-order delay partial differential equations. Partial Differential Equations in Applied Mathematics. 7: 100513.

Gouder, P. M., Kolli, V. H., Page, Md. H., Chavaraddi, K. B. and Chandaragi, P. (2022). The Homotopy Perturbation Method to Solve a Wave Equation. Communications in Mathematics and Applications. 13(2): 691–701.

Hamza, M. M., Suleiman, B. A., Ahmad, S. K. and Tasiu, A. R. (2024). Nonlinear-mixed convection flow with variable thermal conductivity impacted by asymmetric/symmetric heating/cooling conditions. Arabian Journal for Science and Engineering. https://doi.org/10.1007/s13369-024-08757-5

Hassan, A., Hussain, A., Arshad, M., Gouadria, S., Awrejcewicz, J., Galal, A. M., Alharb, F. M. and Eswaramoorthi, S. (2022). Insight into the significance of viscous dissipation and heat generation/absorption in magneto-hydrodynamic radiative Casson fluid flow with first-order chemical reaction. Frontiers in Physics. 10: https://doi.org/10.3389/fphy.2022.920372

Jha, B. K. and Aina, B. (2017). Impact of Induced Magnetic Field on MHD Mixed Convection Flow in Vertical Microchannel Formed by Non-Conducting and Conducting Infinite Vertical Parallel Plates. Journal of Nanofluids. 6: 960 – 970. https://doi.org/10.1166/jon.2017.1376

Jha, B. K. and Samaila, G. (2022). Mixed convection flow from a convectively heated vertical porous plate with combined effects of suction/injection, internal heat generation and nonlinear thermal radiation. Proc IMechE Part E: Journal Process Mechanical Engineering. 1–10. https://doi.org/10.1177/09544089221116963.

Jassim, H. K. and Mohammed, M. G. (2021). Natural homotopy perturbation method for solving nonlinear fractional gas dynamics equations. Int. J. Nonlinear Anal. Appl. 12(1): 812 – 820. http://dx.doi.org/10.22075/IJNAA.2021.4936

Kaita, I. H., Zayyanu, S. Y., Mas'ud, L., Hamsiu, A., Abdullahi, U. and Auwal, D. M. (2024). Heat and mass transfer flow in a channel filled with porous medium in the presence of variable thermal conductivity. FUDMA Journal of Sciences. 8(2): 225 – 234. https://doi.org/10.33003/fjs-2024-0802-223.

Khaleghizadeh, S. (2022). Homotopy perturbation method with the help of Adomian decomposition method for nonlinear problems. Mathematical Analysis and its Contemporary Applications. 4(1): 45 – 51.

Kumar, K. T., Kalyan, S., Kandagal, M., Tawade, M. J., Khan, U., Eldin, S. M., Chohan, J. S., Elattar, S. and Abed, A. M. (2023). Influence of heat generation/absorption on mixed convection flow field with porous matrix in a vertical channel. Case Studies in Thermal Engineering. 47: 103049. 1 – 18. https://doi.org/10.1016/j.csite.2023.103049

Mishra, S., Swain, K. and Dalai, ND. R. (2023). Joule heating and viscous dissipation effects on heat transfer of hybrid nanofluids with thermal slip . Iranian Journal of Science and Technology, Transactions of Mechanical Engineering. https://doi.org/10.1007/s40997-023-00681-7

Nabwey, H. A., Ashraf, M., Rashad, A. M. Chamkha, A. J. (2024). A review on magnetic permeability in heat and fluid flow characteristics: Applications in magnetized shielding. AIP Advances. 14, 120701

Omokhuale, E. and Dange M. S. (2023). Natural Convection Couette Flow in the Presence of Magnetic Field and Thermal Property. International Journal of Science for Global Sustainability. 9(2): 10 – 20. https://doi.org/10.57233/ijsgs.v9i2.453.

Oni, M. O. and Jha, B. K. (2019). Heat Generation/Absorption Effect on natural convection flow in a vertical annulus with time-periodic boundary conditions. Journal of Aircraft and Spacecraft Technology. 3: 183 – 196. https://doi.org/10.3844/jastsp.2019.183.196

Oni, M. O. and Jha, B. K. (2023). Heat generation/absorption effect on mixed convection flow in a vertical channel filled with a nanofluid: Exact solution. Journal of Oil and Gas Research Reviews. 3(1): 1 – 14.

Ramesh, K. (2018). Effects of viscous dissipation and Joule heating on the Couette flow of a Jeffrey fluid with slip boundary conditions. Propulsion and Power Research. 3(4): 329 – 341. https://doi.org/10.1016/j.jppr.2018.11.008

Razaa, Q., Qureshi, Z. A., Alkarni, S., Ali, B., Zain, A., Asogwa, K. K., Shah, N. A., and Yookh, S. (2023). Significance of viscous dissipation, nanoparticles, and Joule heat on the dynamics of water: The case of two porous orthogonal disk. Case Studies in Thermal Engineering. 45: 103008.

Sekhar, K. VC. (2023). Unsteady MHD free convection flow of a second grade casson fluid with ramped wall temperature. Journal of Advanced Research in Fluid Mechanics and Thermal Sciences. 111(1): 80 – 95. https://doi.org/10.37934/arfmts.111.1.8095

Shabiha, N., Tamizharasi, R. (2025). Influence of induced magnetic field, electric load and viscous dissipation on electro-hydromagnetic Jeffrey fluid flowing in an insulated vertical channel: An application of electric power generation. Results in Engineering. 26: 104963. https://doi.org/10.1016/j.rineng.2025.104963

Sobamowo, M. G. (2023). Direct applications of homotopy perturbation method for solving nonlinear algebraic and transcendental equations. International Journal of Petrochemical Science & Engineering. 6(1): 10 – 22.

Srisailam, B., Reddy, K. S., Narender, G. and Malga, B. S. (2023). The Effect of viscous dissipation and chemical reaction on the flow of MHD nanofluid. Journal of Advanced Research in Fluid Mechanics and Thermal Sciences. 107(2): 150 – 170. https://doi.org/10.37934/arfmts.107.2.150170

Tafida, M. K., Umar, A. M. and Umar, L. (2023). Magnetohydrodynamics free Convection Couette flow and heat transfer through a vertical porous plate with heat generation and absorption effect. Dutse Journal of Pure and Applied Sciences. 9(2a): 133 – 145. https://dx.doi.org/10.4314/dujopas.v9i2a.13

Tafida, M. K., Umar, A. M. and Usman, M. I. (2024). Analytical study on fully developed mixed convection Couette flow in a vertical channel with viscous dissipation effect. FUDMA Journal of Sciences. 8(5): 193 – 200. DOI: https://doi.org/10.33003/fjs-2024-0805-2652

Tafida, M. K. and Tajuddeen, A. (2024). Homotopy perturbation method for analyzing the effect of viscous dissipation on steady natural convection Couette flow with convective boundary conditions. International Journal of Fluid Mechanics and Thermal Sciences. 10(3), 45 – 56. https://doi.org/10.11648/j.ijfmts.20241003.11

Usman, A. (2024). Examinations of viscous dissipation, magnetic field and thermal radiation on the systematic flow of Casson fluid with gyrotactic microorganisms. ITM Web of Conferences 67: 01049. https://doi.org/10.1051/itmconf/20246701049

Waini, I., Alabdulhady, S., Ishak, A. and Pop, I. (2023). Viscous dissipation effects on hybrid nanofluid flow over a non-linearly shrinking sheet with power-law velocity. Heliyon. 9: e20910.

Zigta, B. (2022). Thermal Radiation, chemical reaction and viscous dissipation effects on MHD mixed convection flow of micro polar fluid with stretching surface in the presence of heat generation/absorption. Journal of Fluid Dynamics. 3(2), 45 – 64. https://doi.org/10.36959/717/662.